© 2017. Published by The Company of Biologists Ltd | Journal of Cell Science (2017) 130, 2551-2563 doi:10.1242/jcs.200642

RESEARCH ARTICLE

HIRA deficiency in muscle fibers causes hypertrophy and susceptibility to oxidative stress

Nicolas Valenzuela[1], Benjamin Soibam[2], Lerong Li[3], Jing Wang[3], Lauren A. Byers[4], Yu Liu[1], Robert J. Schwartz[1,5] and M. David Stewart[1,5,*]

ABSTRACT

Nucleosome assembly proceeds through DNA replication-coupled or replication-independent mechanisms. For skeletal myocytes, whose nuclei have permanently exited the cell cycle, replication-independent assembly is the only mode available for chromatin remodeling. For this reason, any nucleosome composition alterations accompanying transcriptional responses to physiological signals must occur through a DNA replication-independent pathway. HIRA is the histone chaperone primarily responsible for replication-independent incorporation of histone variant H3.3 across gene bodies and regulatory regions. Thus, HIRA would be expected to play an important role in epigenetically regulating myocyte gene expression. The objective of this study was to determine the consequence of eliminating HIRA from mouse skeletal myocytes. At 6 weeks of age, myofibers lacking HIRA showed no pathological abnormalities; however, genes involved in transcriptional regulation were downregulated. By 6 months of age, myofibers lacking HIRA exhibited hypertrophy, sarcolemmal perforation and oxidative damage. Genes involved in muscle growth and development were upregulated, but those associated with responses to cellular stresses were downregulated. These data suggest that elimination of HIRA produces a hypertrophic response in skeletal muscle and leaves myofibers susceptible to stress-induced degeneration.

KEY WORDS: HIRA, Muscle, H3.3, Hypertrophy, Histone, Chromatin

INTRODUCTION

Eukaryotic cells have two modes of nucleosome assembly – DNA replication-coupled chromatin assembly and DNA replication-independent chromatin assembly. Replication-coupled chromatin assembly occurs in proliferating cells during S phase, whereas replication-independent chromatin assembly occurs outside of S phase and is the only mode of nucleosome assembly available to non-proliferating cells (for recent reviews, see Burgess and Zhang, 2013; Gurard-Levin et al., 2014; Venkatesh and Workman, 2015). Myocytes, like many terminally differentiated cell types, have permanently exited the cell cycle. Thus, replication-independent chromatin assembly is the only mechanism available for these cells to alter nucleosome composition (Rai and Adams, 2012).

The canonical core histones are synthesized during S phase and are utilized for replication-coupled chromatin assembly. In contrast, histone variants are synthesized throughout the cell cycle and utilized for both replication-coupled and replication-independent chromatin assembly. Histone variants confer unique properties to chromatin, establishing unique chromatin environments that are either permissive or restrictive to transcription (reviewed in Gaume and Torres-Padilla, 2015; Zink and Hake, 2016).

Myocytes express a unique gene program that defines their individual cell type. This gene program is epigenetically defined by a specific genomic profile of histone post-translational modifications and histone variants. The mechanisms that define these epigenetic profiles are complex. Myocytes must also adjust gene expression in response to intracellular and extracellular cues. Thus, they must alter the histone modifications and histone variants associated with specific loci in a DNA replication-independent manner.

Histone H3.3, the predominant free H3 isoform available for replication-independent chromatin assembly, has important functions in the epigenetic regulation of transcription (Ahmad and Henikoff, 2002a; Hamiche and Shuaib, 2012). Histone H3.3 is enriched at promoter and enhancer regions of actively transcribed genes. In genic regions, it is the primary H3 isoform to be modified by the 'active' marks of acetylation and lysine 4 methylation (Ahmad and Henikoff, 2002b). In a seemingly opposing role, it leads to the compaction of constitutive heterochromatin regions such as telomeres and pericentric heterochromatin, where it is modified by lysine 9 trimethylation (Drane et al., 2010; Goldberg et al., 2010; Lewis et al., 2010; Udugama et al., 2015; Wong et al., 2009). Thus, H3.3 plays an active role in defining the epigenetic landscape and therefore the gene expression program of any given cell type.

HIRA is the chaperone primarily responsible for replication-independent incorporation of histone variant H3.3 at genic loci (Goldberg et al., 2010; Tagami et al., 2004). HIRA-mediated H3.3 deposition occurs across gene bodies after passage of RNA polymerase II and at promoter/enhancer regions where it facilitates a dynamic chromatin environment that increases accessibility to trans-acting factors (Banaszynski et al., 2013; Schwartz and Ahmad, 2005). HIRA indirectly facilitates assembly of senescence-associated heterochromatin foci through an unknown mechanism (Zhang et al., 2007, 2005). HIRA is also important for transcriptional restart after transcription-coupled nucleotide excision repair (Adam et al., 2013). The *HIRA* gene is of clinical importance due to its location within the critical region of the 22q11.2 deletion – the genetic cause of DiGeorge/velocardiofacial syndrome (OMIM 188400) (Carlson et al., 1997; Halford et al.,

[1]Department of Biology and Biochemistry, University of Houston, Houston, TX 77204, USA. [2]Department of Computer Science and Engineering Technology, University of Houston-Downtown, Houston, TX 77002, USA. [3]Department of Bioinformatics and Computational Biology, The University of Texas MD Anderson Cancer Center, Houston, TX 77030, USA. [4]Department of Thoracic Head & Neck Medical Oncology, The University of Texas MD Anderson Cancer Center, Houston, TX 77030, USA. [5]Stem Cell Engineering Department, Texas Heart Institute at St. Luke's Episcopal Hospital, Houston, TX 77030, USA.

*Author for correspondence (dstewart@uh.edu)

M.D.S., 0000-0002-4794-6843

Received 11 December 2016; Accepted 5 June 2017

Journal of Cell Science (2017) 130, 2551-2563 doi:10.1242/jcs.200642

1993). Because replication-independent chromatin assembly is the only available mode of chromatin assembly in postmitotic cells like myocytes, HIRA would be expected to play an important role in epigenetically defining gene expression and in adjusting gene expression in response to physiological cues. For example, skeletal myocytes upregulate and downregulate expression of specific gene sets in response to nerve-evoked electrical activity, hypertrophy and atrophy signals, metabolism demands, and cellular stresses such as DNA damage and oxidative stress. It would be expected that these gene expression alterations be impacted by replication-independent chromatin assembly of histone variants.

The objective of this study was to determine the consequence of ablating HIRA-mediated chromatin assembly within skeletal myocytes (myofibers), a terminally differentiated postmitotic cell type. This was accomplished in mice using a conditional knockout approach, where *Hira* was inactivated at the myotube/myofiber stage by using *Myf6-cre*. Our data indicate that HIRA deficiency produces a hypertrophic response in skeletal muscle and leaves myofibers susceptible to stress-induced degeneration.

RESULTS

Confirmation of muscle-specific Hira CKO using Myf6-cre

The $Hira^{flox}$ allele contains *loxP* sites flanking exon 4. Elimination of exon 4 from *Hira* mRNA transcripts was tested by reverse transcription PCR using primers flanking exon 4. The wild-type transcript was detected in wild-type and *Hira* conditional knockout (CKO) muscles. Deleted exon 4 transcripts were only detected in *Hira* CKO muscles (Fig. S1A).

Our genetic cross included the $Rosa26^{YFP}$ allele. Thus, cells subjected to cre-induced recombination could be identified by YFP fluorescence. YFP was absent from wild-type (*Myf6-cre*-negative) muscles, but present throughout the muscles of control and *Hira* CKO mice, both of which contained the $Myf6^{cre}$ allele (Fig. S1B). These results confirm correct expression of the skeletal muscle-specific cre driver and functionality of the *Hira* CKO allele.

Lower body weight and less fat mass by 6 months of age

General measurements of body weight, size, lean and fat mass (body composition), and the mass of individual muscles were obtained at 6 weeks and 6 months of age for male mice. At 6 weeks of age, control and *Hira* CKO littermates appeared visually similar (Fig. 1A) and there was no effect of the *Hira* CKO on any of these parameters (Fig. 1B–H). However, by 6 months of age, *Hira* CKO mice visually appeared leaner (Fig. 1J) and weighed less than control littermates (Fig. 1K). Body composition analysis by MRI revealed that *Hira* CKO males exhibited more lean mass (Fig. 1M) and less fat mass (Fig. 1N) than their control littermates. There was no difference in tibia length (Fig. 1L), nor were there differences in the wet masses of individual muscles, including the gastrocnemius, soleus or tibialis anterior (TA) (Fig. 1O–Q). Because body size and muscle masses were not significantly different, we attribute the difference in body weight at 6 months of age to be due to a reduction in total fat mass. Strength was measured by a four-paw grip strength test for male mice. At both 6 weeks and 6 months of age, control and *Hira* CKO males exhibited similar grip strength when normalized to lean mass (Fig. 1I,R).

Myofiber hypertrophy and regeneration

Muscle histology was examined by H&E staining. At 6 weeks of age, there was no obvious pathology in the fast-twitch TA muscle (Fig. 2A,B). However, by 6 months of age, the *Hira* CKO TA exhibited what appeared to be a broad variation in fiber sizes and many fibers with central nuclei (Fig. 2F,G). These observations were subsequently quantified separately for the medial and lateral regions of the TA. Generally, the lateral TA (lateral to the TA tendon/exterior region) has larger fiber sizes and more fast glycolytic (type IIb) fibers than the medial TA (medial to the TA tendon/interior region). At 6 weeks of age, there was no difference in the percentage of central nuclei in the lateral or medial TA (Fig. 2C). However, by 6 months of age, ∼15% of fibers in the *Hira* CKO TA exhibited central nuclei (Fig. 2H). The distribution of fiber sizes was quantified by measuring the minimum Feret diameter of individual fibers. At 6 weeks of age, there was no difference in the distribution of fiber sizes within the medial TA (Fig. 2D); however, myofiber hypertrophy was detectable in the lateral TA (Fig. 2E). At 6 months of age, *Hira* CKO mice exhibited a broader distribution of fiber sizes compared to that in control animals, including increased numbers of both hypertrophic and hypotrophic fibers in both the medial and lateral TA (Fig. 2I,J). The increased percentage of small fibers in the *Hira* CKO at 6 months of age likely reflects regeneration, as evident by the high number of fibers with central nuclei. Collectively, these data indicate that hypertrophy and regeneration are pathological consequences of loss-of-function *Hira* mutations in myofibers.

We performed identical experiments using the slow-twitch soleus muscle. Similar to the TA, there were no obvious pathological peculiarities at 6 weeks of age (Fig. 3A,B). By 6 months of age, a few fibers with central nuclei were observed in the *Hira* CKO (Fig. 3E,F). These visual observations were confirmed by counting the percentage of fibers with central nuclei. There was no significant difference at 6 weeks of age (Fig. 3C); however, by 6 months of age, ∼3% of the fibers in the *Hira* CKO soleus exhibited central nuclei (Fig. 3G). Unlike the TA, we found no difference in the myofiber minimum Feret diameter at 6 weeks (Fig. 3D) or 6 months (Fig. 3H) of age. Thus, the hypertrophic response to loss of HIRA appears to much more profoundly affect fast-twitch muscles.

Few young myofibers but broad upregulation of muscle genes

Our histological findings led us to test the hypothesis that loss of HIRA promotes hypertrophy, but these fibers eventually die leading to increased myofiber regeneration. First, we assayed the percentage of newly formed fibers positive for embryonic myosin heavy chain (eMyHC; also known as MYH3) in the TA. No eMyHC-positive fibers were observed in control TA sections at either 6 weeks or 6 months of age (Fig. 4A,C). In contrast, a few eMyHC-positive fibers were observed in *Hira* CKO TA sections at 6 weeks and 6 months of age (Fig. 4B,D). These observations were quantified and reported as the percentage of eMyHC-positive fibers per TA section. The results of this analysis showed no statistical difference between controls and *Hira* CKOs at 6 weeks (Fig. 4E) or 6 months (Fig. 4F) of age. This result is likely due to the low numbers of eMyHC-positive fibers and several CKO sections where no eMyHC-positive fibers were detectable.

Gene expression analyses supported the idea of increased myofiber regeneration activity in *Hira* CKO muscle. Consistent with the presence of eMyHC-positive fibers only in the *Hira* CKO, expression of the *eMyHC* (*Myh3*) gene was significantly higher within the *Hira* CKO TA at 6 months of age as determined by real-time quantitative PCR (qPCR) (Fig. 4G). Next, we compared expression of major regeneration/developmental genes between control and *Hira* CKO TA at 6 months of age by microarray analysis. The results of this analysis showed upregulation of *Myod1*, *Myog*, *Myh3* (eMyHC), *Myh8* (fetal MyHC), *Myh7* (slow MyHC)

Journal of Cell Science (2017) 130, 2551-2563 doi:10.1242/jcs.200642

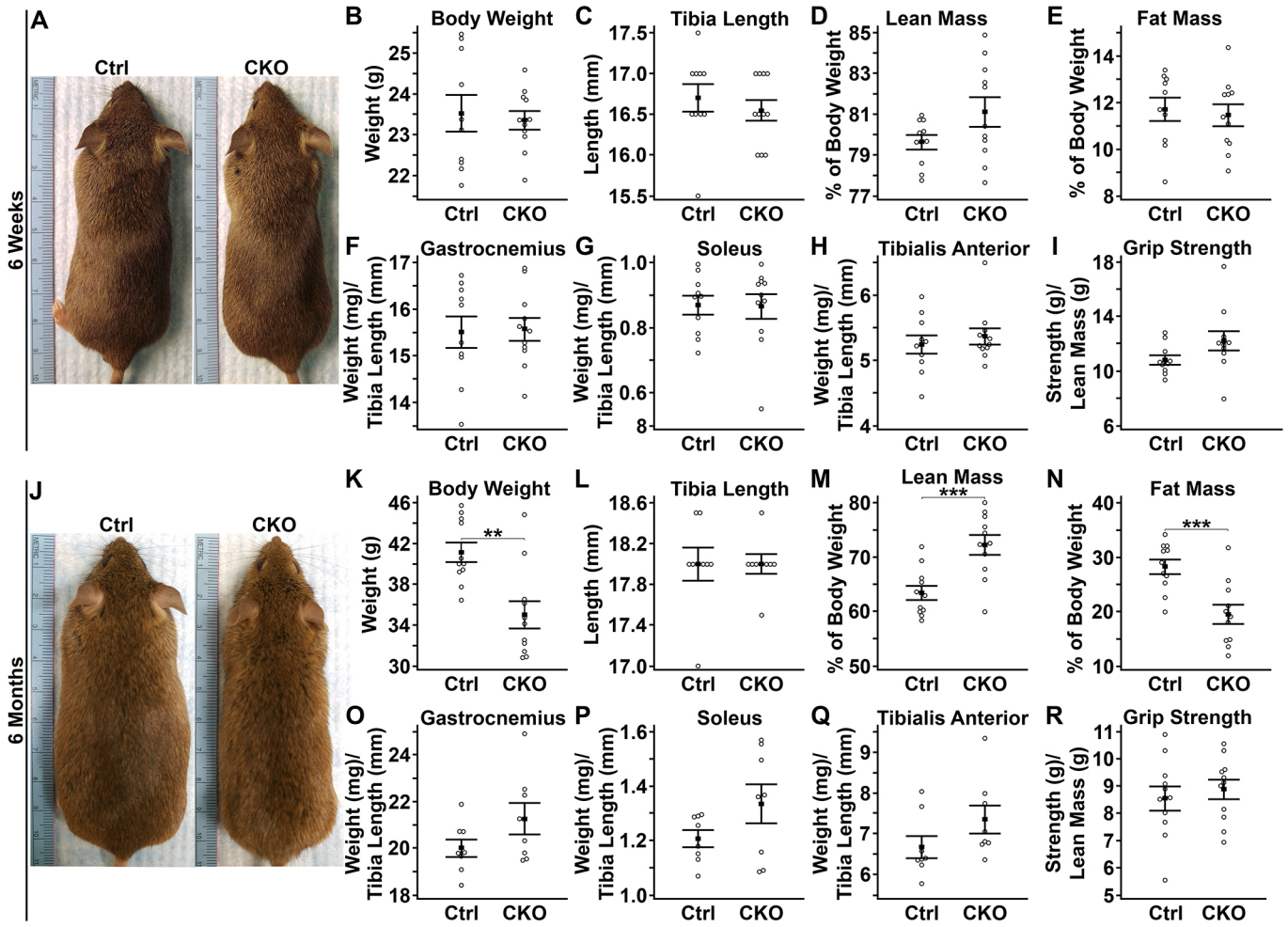

Fig. 1. Lower body weight and less fat mass by 6 months of age. Body composition (percentage lean and fat mass) was obtained by MRI. Muscle wet weights were the combined weight of left and right pairs. No significant differences were observed at 6 weeks of age for any measurements [*n*=10 control (Ctrl) and 11 CKO animals/group for all experiments] (A–I). At 6 months of age, *Hira* CKO mice appeared thinner (J), exhibited reduced body weight (K), increased lean mass (M) and decreased fat mass (*n*=11 animals/group) (N). No difference was observed for tibia length (L) or individual muscle weights (O–Q) (*n*=8 animals/group). Grip strength was not different at either 6 weeks (I) or 6 months (R) of age. Data were normalized to lean mass (*n*=10 Ctrl and 11 CKO animals/group at 6 weeks, *n*=11 animals/group at 6 months). ***P*<0.01, ****P*<0.001 (Student's *t*-test). Error bars show the mean±s.e.m.

and *Smyd1*. No significant difference was found for *Myf5* and *Myf6* (Fig. 4H). Furthermore, many differentially expressed genes categorized under the Gene Ontology terms 'sarcomere' (GO 0030017) (Fig. 4I), 'sarcolemma' (GO 0042383) (Fig. 4J) or 'striated muscle development' (GO 0014706) (Fig. 4K) were upregulated in the *Hira* CKO TA at 6 months of age. Collectively, these data indicate that loss of HIRA activates muscle growth and developmental gene expression.

Alterations in gene expression

Elimination of HIRA from myofibers had significant consequences on gene expression as determined by microarray analyses using RNA extracted from TA muscles at 6 weeks and 6 months of age. Appropriate grouping of control and *Hira* CKO data was confirmed by principal component analysis (PCA) (Fig. S2A, S3A) and clustering analyses (Fig. S2B, S3B). We found 4684 genes to be upregulated and 4367 genes to be downregulated in the *Hira* CKO at 6 weeks of age. At 6 months of age, 3669 genes were upregulated and 3910 genes were downregulated in the *Hira* CKO as compared to control animals. Gene Ontology analysis was used to identify pathways particularly affected by the absence of HIRA (Table 1). At 6 weeks of age (prior to pathological defects), we primarily found downregulation of genes involved in transcription, transcriptional regulation and chromatin. This observation is consistent with the function of HIRA in chromatin assembly. By 6 months of age, we found altered expression (up and down) of many genes involved in metabolic processes, upregulation of muscle growth and developmental genes, and downregulation of cellular stress response genes (some of which were also downregulated at 6 weeks). Thus, downregulation of genes involved in transcription preceded pathological abnormalities, which were not detected until 6 months of age.

Impaired sarcolemmal integrity and oxidative stress-induced degeneration

We previously determined the physiological consequence of eliminating HIRA from cardiomyocytes (Valenzuela et al., 2016). Similar to skeletal muscle, CKO of *Hira* from cardiomyocytes using *αMHC-cre* resulted in hypertrophy. We also found that hypertrophic cardiomyocytes in the *Hira* CKO became fragile, and susceptible to sarcolemmal perforation and oxidative stress. Thus, we tested whether *Hira* CKO myofibers also exhibited sarcolemmal damage

Journal of Cell Science (2017) 130, 2551-2563 doi:10.1242/jcs.200642

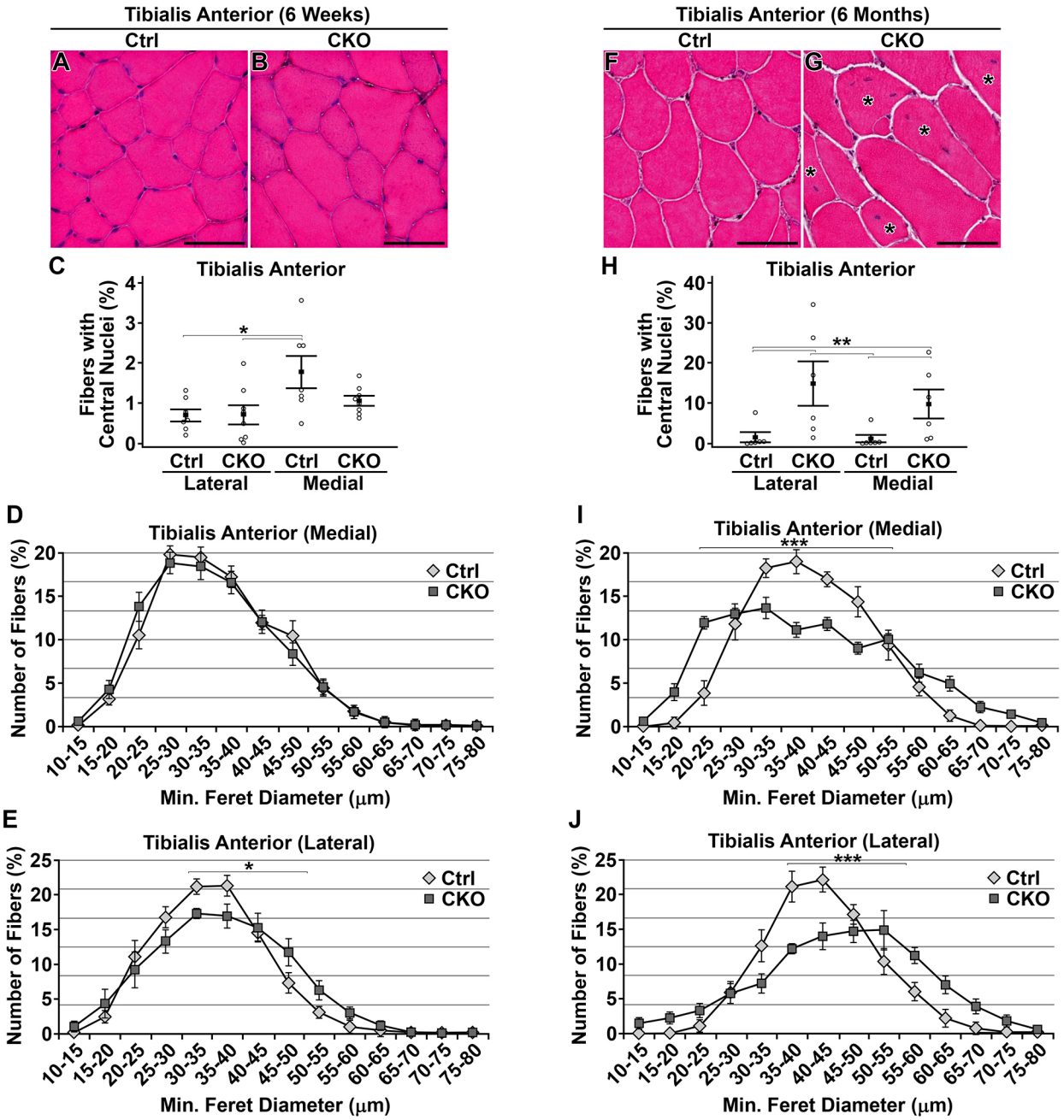

Fig. 2. Myofiber hypertrophy and regeneration in the TA. (A–E) Data from 6-week-old male mice. (A,B) TA cryosections stained with H&E. No particularities were noted. (C) The medial TA contained more fibers with central nuclei that the lateral TA, but there was no difference between control and *Hira* CKO mice. **P*<0.05 [Kruskal–Wallis test, *n*=7 control (Ctrl) and 8 CKO animals/group]. (D,E) Quantification of myofiber size by minimum Feret diameter measurements for the medial (D) and lateral (E) TA muscle. No difference was seen in myofiber size for the medial region (D). The lateral TA of *Hira* CKO mice exhibited increased hypertrophic myofibers (E). **P*<0.05 (two-way ANOVA, *n*=7 Ctrl and 8 CKO animals/group). (F–J) Data from 6-month-old male mice. (F,G) TA cryosections stained with H&E. *Hira* CKO muscle exhibited widespread myofibers with central nuclei (asterisks) (G). (H) *Hira* CKO mice exhibited more myofibers with central nuclei in both the lateral and medial TA. ***P*<0.01 (Kruskal–Wallis test, *n*=6 animals/group). (I,J) Quantification of myofiber size by minimum Feret diameter measurements for the medial (I) and lateral (J) TA. *Hira* CKO mice exhibited increased numbers of small and large fibers within both the medial and lateral regions. ****P*<0.001 (two-way ANOVA, *n*=6 animals/group). Error bars show the mean±s.e.m. Scale bars: 50 µm.

and signs of oxidative stress. Sarcolemmal perforation was assayed by uptake of Evans Blue dye to the TA at 6 months of age. No myofibers positive for Evans Blue dye were detectable in control animals (Fig. 5A–C) (*n*=4). In contrast, Evans Blue-positive myofibers were readily detectable in *Hira* CKO animals (*n*=3) either by stereoimaging (Fig. 5D) or by far-red fluorescence in cryosections (Fig. 5E,F). These results are consistent with the impaired sarcolemmal integrity observed in cardiomyocytes lacking HIRA. A search of our microarray data for sarcolemmal genes (GO 0042383) that were downregulated in *Hira* CKO muscle at both 6 weeks and 6 months of age revealed 19 genes (Fig. 5G). Of these genes, deficiencies in phospholemman (*Fxyd1*), utrophin (*Utrn*), filamin C (*Flnc*), integrin α7 (*Itga7*), popeye domain-containing 2 (*Popdc2*), sarcoglycan α (*Sgca*), sarcoglycan β (*Sgcb*) or

Journal of Cell Science (2017) 130, 2551-2563 doi:10.1242/jcs.200642

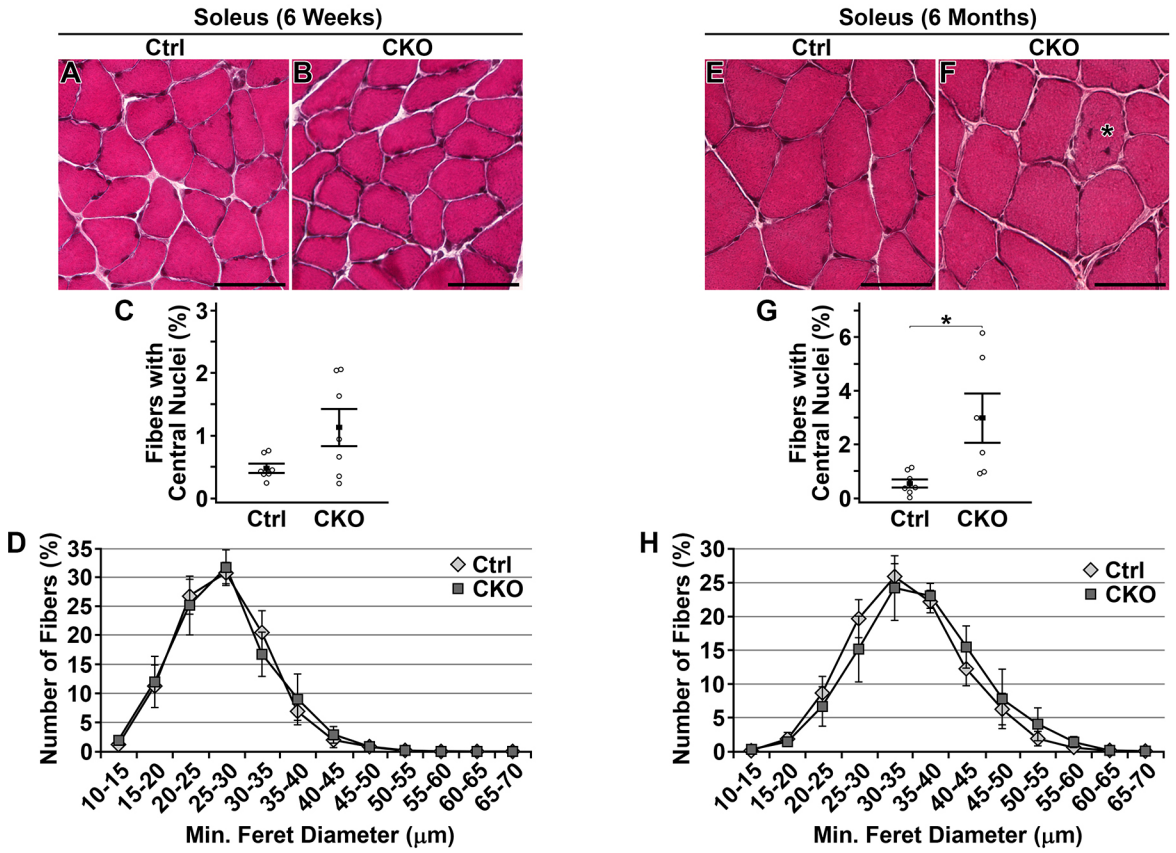

Fig. 3. Modest pathology in the soleus. (A–D) Data from 6-week-old male mice. (A,B) Soleus cryosections stained with H&E. No particularities were noted. (C) No difference was found in the percentage of myofibers with central nuclei (Student's *t*-test, *n*=7 animals/group). (D) No difference was found in myofiber size (minimum Feret diameter) (two-way ANOVA, *n*=7 animals/group). (E–H) Data from 6-month-old male mice. (E,F) Soleus cryosections stained with H&E. *Hira* CKOs appeared similar to controls except for a few myofibers with central nuclei (asterisk in F). (G) Quantification of the percentage of myofibers with central nuclei. **P*<0.05 [Student's *t*-test, *n*=7 control (Ctrl) and 6 CKO animals/group]. (H) Quantification of myofiber size by minimum Feret diameter measurements. No difference was found in myofiber size (two-way ANOVA, *n*=7 Ctrl and 6 CKO animals/group). Error bars show the mean±s.e.m. Scale bars: 50 µm.

dystrobrevin α (*Dtna*) are likely contributors to dystrophic myofibers.

The relative abundance of reactive oxygen species (ROS) in the TA muscle of 6-month-old mice was determined by assessing the presence of 3-nitrotyrosine, a stable end-product of oxidation by reactive nitrogen species. Similar to what was observed in *Hira* CKO cardiomyocytes, small numbers of nitrotyrosine-positive myofibers were detectable in *Hira* CKO muscles (Fig. 5J,K), but not in controls (Fig. 5H,I). Nitrotyrosine-positive fibers were typically found in the lateral region of the TA (Fig. 5L) as two varieties – large fibers such as illustrated in Fig. 5J or what appeared to be degenerating fibers as illustrated in Fig. 5K. Evans Blue-positive fibers exhibited similar morphologies (Fig. 5F). These data support the idea that large hypertrophic fibers in the *Hira* CKO succumb to oxidative stress and degenerate, thereby stimulating regeneration.

Microarray analysis of gene expression within the TA at 6 months of age revealed enrichment in the *Hira* CKO of downregulated differentially expressed genes falling under the Gene Ontology term 'response to oxidative stress' (GO 0006979) (Fig. 5M). This is similar to what was observed in *Hira* CKO cardiomyocytes and suggests impaired response to oxidative stress in the absence of HIRA.

To further test the idea that loss of HIRA impairs cellular stress responses, we performed a reverse phase protein array (RPPA) using protein extracts from the TA of 6-month-old mice. This specific RPPA has been repeatedly used to screen tumor samples for alterations in cell cycle effectors and regulators of the DNA damage response (Byers et al., 2012). We thought it useful because it contains antibodies against many checkpoint proteins activated in response to DNA damage as well as effectors of hypertrophy in muscle. Of the 181 antibodies on the array, 18 targets were identified to be differentially expressed ($P<0.05$) (Fig. 5N; Fig. S4). Four proteins showed higher expression in the *Hira* CKO, including AKT (antibody recognizes all isoforms) and the AKT phosphorylation target WEE1 phosphorylated at S642 (denoted WEE1.pS642) (Fig. 5O). A total of 14 proteins were of lower relative abundance in the *Hira* CKO, including caspase-3, XIAP, MDM2 phosphorylated at S166 (denoted MDM2.pS166) and caspase-7, all of which would reduce atrophy and/or promote hypertrophy. Several effectors of the DNA damage response were reduced in the *Hira* CKO, including CHK2 T68 (CHK2.pT68; CHK2 is also known as CHEK2), JNK2, ATR, ATM phosphorylated at S1981 (ATM.pS1981) and MCL1 (Fig. 5O). The proteins identified as differentially expressed in the RPPA showed consistency with our microarray data. Specifically, microarray analysis identified *Akt* and *Wee1* to be upregulated, and *Xiap*, *Chek2*, *Mapk9* (also known as *Jnk2*), *Atr*, *Casp7*, *Atm*, *Mcl1* and *Elk1* to be downregulated in *Hira* CKO skeletal muscle, heart or both. These data further support the idea that loss of HIRA impairs cellular responses to oxidative stress.

Journal of Cell Science (2017) 130, 2551-2563 doi:10.1242/jcs.200642

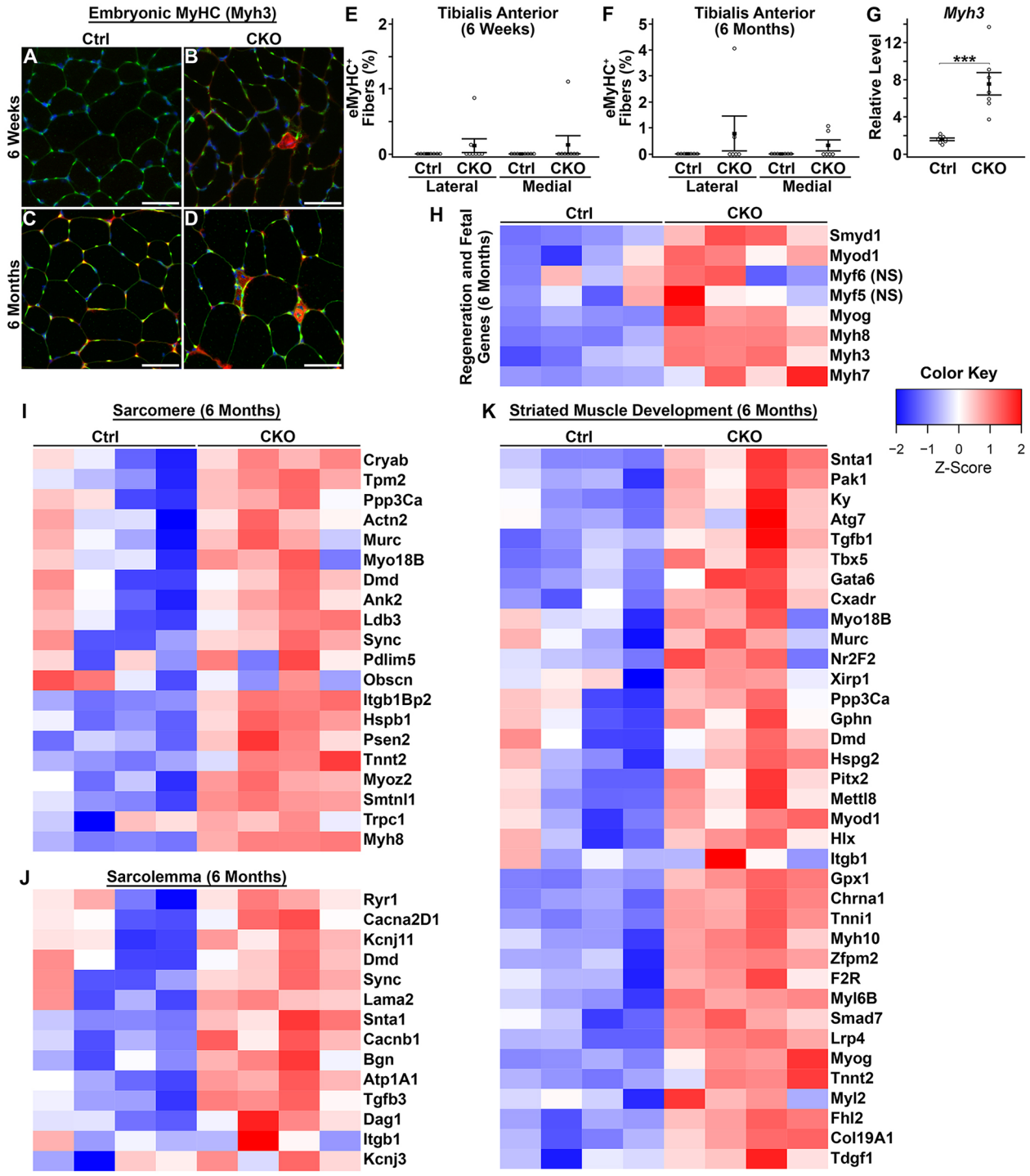

Fig. 4. Few young myofibers, but broad upregulation of muscle genes. (A–D) TA cryosections immunostained for eMyHC at 6 weeks (A,B) or 6 months (C,D) of age. Red, eMyHC; green, membranes stained with WGA-488; blue, nuclei stained with DAPI. eMyHC-positive fibers were absent from control animals, but detectable in some *Hira* CKO mice. (E,F) Quantification of the percentage of eMyHC-positive myofibers in medial and lateral regions of the TA at 6 weeks [*n*=7 control (Ctrl) and 8 CKO animals/group] (E) and 6 months (*n*=6 animals/group) (F) of age. Although eMyHC-positive myofibers were only detected in *Hira* CKO mice, their numbers were very low and there was no statistically significant difference between controls and *Hira* CKOs (6 weeks, *P*=0.35; 6 months, *P*=0.21; Kruskal–Wallis test). (G) qPCR gene expression assay for *Myh3* (*eMyHC*) at 6 months of age. *Myh3* expression was upregulated in *Hira* CKO muscle. ***$P<0.001$ (Student's *t*-test, *n*=8 Ctrl and 7 CKO animals/group). (H–K) Genes associated with regeneration or fetal development were mostly upregulated in *Hira* CKO muscle; however, no difference was detected for *Myf5* and *Myf6* (H). Many differentially expressed genes associated with sarcomere (I), sarcolemma (J) or striated muscle development (K) were upregulated in *Hira* CKO muscle (*n*=4 animals/group). Error bars show the mean±s.e.m. Scale bars: 50 µm.

More type I fibers

Because *Hira* CKO mice exhibited lower fat mass (Fig. 1N) relative to control littermates, we reasoned that type I fibers (oxidative and slow twitch) may be more abundant in the *Hira* CKO. We tested this idea by immunostaining TA and soleus cryosections obtained from 6-week-old and 6-month-old male mice for slow MyHC and

Journal of Cell Science (2017) 130, 2551-2563 doi:10.1242/jcs.200642

Table 1. Gene Ontology terms associated with differentially expressed genes in skeletal muscle

Rank	GO term (biological processes)	*P*-value	FDR
6 weeks			
Genes downregulated in *Hira* CKO muscle			
1	Negative regulation of cell proliferation	2.55×10^{-7}	1.52×10^{-5}
2	Transcription, DNA-templated	9.29×10^{-7}	3.96×10^{-5}
3	Transport	1.90×10^{-6}	7.56×10^{-5}
4	Positive regulation of transcription from RNA polymerase II promoter	3.03×10^{-6}	1.13×10^{-4}
5	Negative regulation of transcription from RNA polymerase II promoter	8.98×10^{-6}	3.15×10^{-4}
6	Negative regulation of protein binding	2.94×10^{-5}	8.36×10^{-4}
7	Covalent chromatin modification	6.82×10^{-5}	1.70×10^{-3}
8	Positive regulation of transcription, DNA-templated	8.79×10^{-5}	1.94×10^{-3}
9	Negative regulation of cell migration	1.37×10^{-4}	2.92×10^{-3}
10	Positive regulation of sequence-specific DNA-binding transcription factor activity	1.70×10^{-4}	3.38×10^{-3}
12	Cellular response to DNA damage stimulus	2.85×10^{-4}	4.53×10^{-3}
Genes upregulated in *Hira* CKO muscle			
1	Intracellular signal transduction	2.16×10^{-4}	5.13×10^{-3}
2	Protein stabilization	2.20×10^{-4}	5.13×10^{-3}
3	Transport	2.40×10^{-4}	5.13×10^{-3}
4	Ribosomal large subunit biogenesis	2.70×10^{-4}	5.38×10^{-3}
5	Transcription, DNA-templated	4.39×10^{-4}	7.15×10^{-3}
6	Protein transport	4.90×10^{-4}	7.30×10^{-3}
7	Translational initiation	4.91×10^{-4}	7.30×10^{-3}
8	Regulation of cysteine-type endopeptidase activity involved in apoptotic process	5.29×10^{-4}	7.54×10^{-3}
9	Regulation of membrane repolarization	8.50×10^{-4}	9.69×10^{-3}
6 months			
Genes downregulated in *Hira* CKO muscle			
1	tRNA metabolic process	3.59×10^{-7}	2.60×10^{-5}
2	Cofactor metabolic process	7.35×10^{-7}	3.88×10^{-5}
3	tRNA processing	1.15×10^{-6}	3.88×10^{-5}
4	Coenzyme metabolic process	2.16×10^{-6}	6.07×10^{-5}
5	ncRNA metabolic process	2.93×10^{-6}	5.49×10^{-4}
6	Oxidation reduction	4.05×10^{-5}	7.32×10^{-4}
7	Cofactor biosynthetic process	6.80×10^{-5}	1.13×10^{-3}
8	Nucleoside metabolic process	1.46×10^{-4}	2.24×10^{-3}
9	ncRNA processing	1.97×10^{-4}	2.77×10^{-3}
10	Angiogenesis	2.13×10^{-4}	2.79×10^{-3}
12	DNA metabolic process	2.85×10^{-4}	3.28×10^{-3}
14	Cellular response to stress	3.42×10^{-4}	3.61×10^{-3}
18	DNA repair	5.11×10^{-4}	4.79×10^{-3}
19	Response to DNA damage stimulus	5.65×10^{-4}	5.03×10^{-3}
25	Chromatin organization	9.13×10^{-4}	6.98×10^{-3}
Genes upregulated in *Hira* CKO muscle			
1	Phosphate metabolic process	4.84×10^{-10}	1.25×10^{-7}
2	Protein localization	3.01×10^{-8}	5.19×10^{-6}
3	Modification-dependent protein catabolic process	1.04×10^{-7}	6.31×10^{-6}
4	Proteolysis involved in cellular protein catabolic process	1.22×10^{-7}	6.31×10^{-6}
5	Cellular protein catabolic process	1.73×10^{-7}	6.31×10^{-6}
6	Protein catabolic process	2.69×10^{-7}	8.13×10^{-6}
7	Cellular macromolecule catabolic process	3.53×10^{-7}	9.31×10^{-6}
8	Establishment of protein localization	6.59×10^{-7}	1.30×10^{-5}
9	Protein transport	6.79×10^{-7}	2.19×10^{-5}
10	Striated muscle cell differentiation	1.64×10^{-6}	2.19×10^{-5}
19	Muscle cell development	4.42×10^{-5}	6.38×10^{-4}
20	Striated muscle cell development	5.52×10^{-5}	6.38×10^{-4}
22	Muscle cell differentiation	6.80×10^{-5}	9.65×10^{-4}
28	Gene silencing	4.19×10^{-4}	3.43×10^{-3}
30	Muscle organ development	5.41×10^{-4}	4.00×10^{-3}
35	Muscle tissue development	8.17×10^{-4}	5.58×10^{-3}
38	Striated muscle tissue development	8.68×10^{-4}	6.04×10^{-3}

For genes that were up- or down-regulated in the *Hira* skeletal muscle CKOs, listed are the top ten biological process gene ontology (GO) terms ranked by *P*-value and notable others with $P<0.0001$ and FDR<0.001. Gene expression data were obtained from a microarray analysis using RNA extracted from the TA at 6 weeks or 6 months of age ($n=4$ animals/group).

determining the percentage of type I fibers. Representative images of TA and soleus sections are presented in Fig. 6A–D and G–J, respectively. For the TA, which in mice normally has very few type I fibers, there was no difference in the percentage of type I fibers at 6 weeks of age; however, as expected, there were slightly more type I fibers in the medial region than the lateral region (Fig. 6E). By 6 months of age, *Hira* CKO TA exhibited significantly more type I fibers in the medial region, but not in the lateral region (Fig. 6F).

Journal of Cell Science (2017) 130, 2551-2563 doi:10.1242/jcs.200642

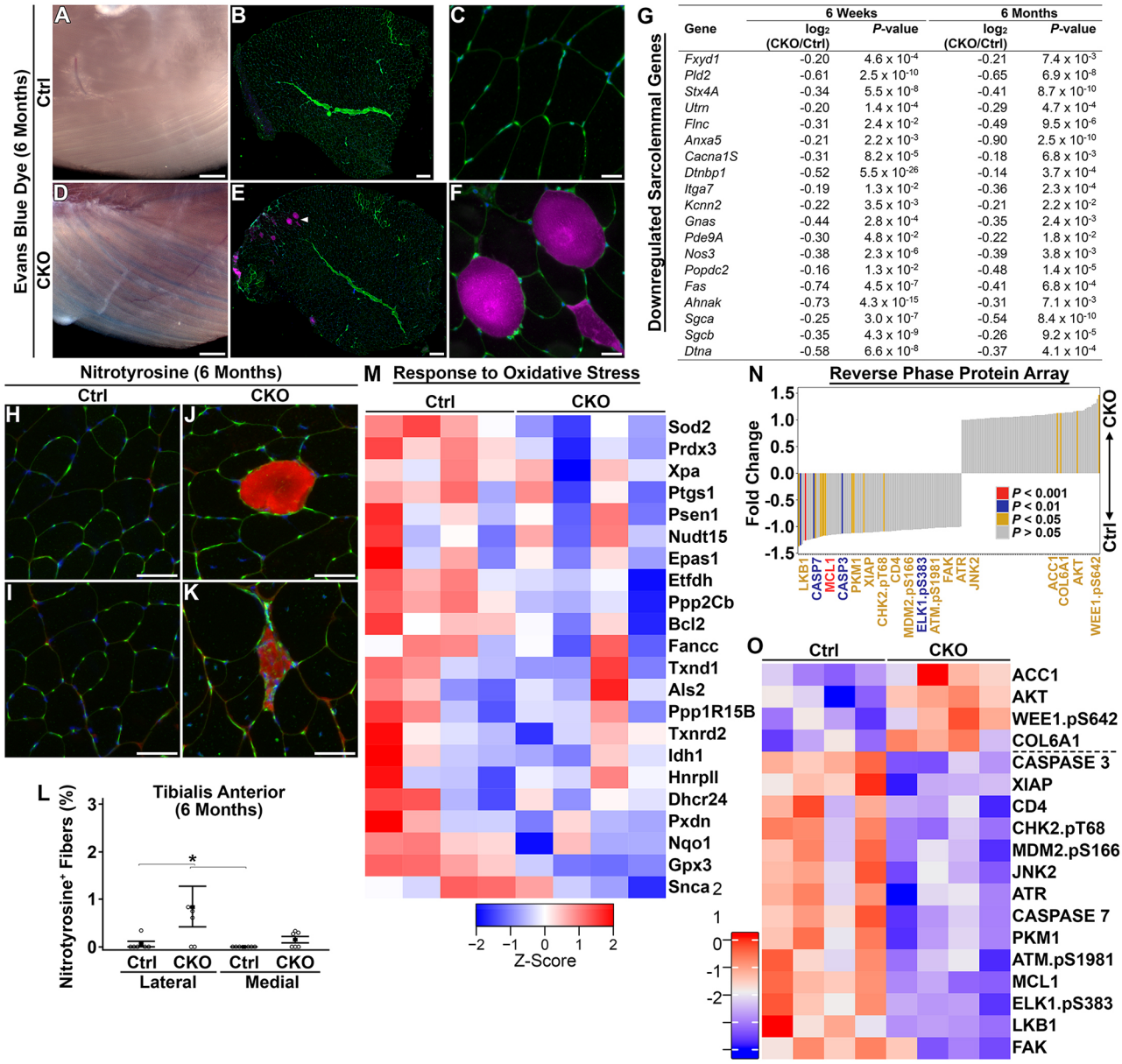

Gene	6 Weeks log2 (CKO/Ctrl)	6 Weeks P-value	6 Months log2 (CKO/Ctrl)	6 Months P-value
Fxyd1	-0.20	4.6×10^{-4}	-0.21	7.4×10^{-3}
Pld2	-0.61	2.5×10^{-10}	-0.65	6.9×10^{-8}
Stx4A	-0.34	5.5×10^{-8}	-0.41	8.7×10^{-10}
Utrn	-0.20	1.4×10^{-4}	-0.29	4.7×10^{-4}
Flnc	-0.31	2.4×10^{-2}	-0.49	9.5×10^{-6}
Anxa5	-0.21	2.2×10^{-3}	-0.90	2.5×10^{-10}
Cacna1S	-0.31	8.2×10^{-5}	-0.18	6.8×10^{-3}
Dtnbp1	-0.52	5.5×10^{-26}	-0.14	3.7×10^{-4}
Itga7	-0.19	1.3×10^{-2}	-0.36	2.3×10^{-4}
Kcnn2	-0.22	3.5×10^{-3}	-0.21	2.2×10^{-2}
Gnas	-0.44	2.8×10^{-4}	-0.35	2.4×10^{-3}
Pde9A	-0.30	4.8×10^{-2}	-0.22	1.8×10^{-2}
Nos3	-0.38	2.3×10^{-6}	-0.39	3.8×10^{-3}
Popdc2	-0.16	1.3×10^{-2}	-0.48	1.4×10^{-5}
Fas	-0.74	4.5×10^{-7}	-0.41	6.8×10^{-4}
Ahnak	-0.73	4.3×10^{-15}	-0.31	7.1×10^{-3}
Sgca	-0.25	3.0×10^{-7}	-0.54	8.4×10^{-10}
Sgcb	-0.35	4.3×10^{-9}	-0.26	9.2×10^{-5}
Dtna	-0.58	6.6×10^{-8}	-0.37	4.1×10^{-4}

Fig. 5. Myofiber degeneration and impaired transcriptional response to oxidative stress. (A–F) Sarcolemmal perforation in the absence of HIRA as determined by uptake of Evans Blue dye. (A,D) Brightfield stereoimages of the TA at 6 months of age. Fibers with sarcolemmal damage showed obvious uptake of Evans Blue dye (D). (B,C,E,F) Cryosections of TA stained with WGA-488. Evans Blue-positive fibers (purple) were present in *Hira* CKO (E,F), but not control animals (B,C) [*n*=3 control (Ctrl) and 4 CKO animals/group]. (G) Sarcolemmal genes downregulated in *Hira* CKO TA at both 6 weeks and 6 months of age. (H–K) Nitrotyrosine-positive fibers were enriched in *Hira* CKO mice. Red, nitrotyrosine; green, membranes stained with WGA-488; blue, nuclei stained with DAPI. (L) Quantification of the percentage of nitrotyrosine-positive myofibers in the medial and lateral regions of the TA at 6 months of age. Nitrotyrosine-positive myofibers were more prevalent in *Hira* CKO mice and enriched in the lateral region of the TA. Error bars show the mean±s.e.m. *P<0.05 (Kruskal–Wallis test, *n*=6 animals/group). (M) Downregulation of genes associated with the response to oxidative stress in *Hira* CKO muscle at 6 months of age as determined by microarray analysis (*n*=4 animals/group). (N) Differentially expressed proteins identified by RPPA using extracts from the TA of 6-month-old mice (*n*=4 animals/group). Of the 181 antibodies on the array, 18 targets were differentially expressed (P<0.05). (O) Heatmap illustrating levels for each differentially expressed protein. Scale bars: 500 µm (A,D) and 50 µm (B,C,E,F,H–K).

Within the soleus, we found significantly more type I fibers in *Hira* CKOs at both 6 weeks and 6 months of age. Similar to what is seen in wild-type mice, the soleus of control mice consisted of ∼40% type I fibers. The soleus of *Hira* CKO mice exhibited ∼50% type I fibers (Fig. 6K,L). Consistent with our analysis of type I fiber abundance, expression of genes encoding slow-twitch muscle contractile proteins was increased in the TA muscle of *Hira* CKO mice at 6 months of age. There was little effect on slow-twitch muscle gene expression at 6 weeks of age (Fig. 6M).

Similarities in differential gene expression between muscle and heart

One of the goals of this project was to improve our understanding of HIRA-regulated muscle gene expression by identifying differentially expressed genes that were common to both cardiomyocyte and skeletal myocyte *Hira* CKOs. 1304 genes were upregulated in both of these two *Hira* CKOs (Fig. 7A). Gene Ontology analysis showed enrichment of genes involved in translation, protein transport and cell proliferation (Fig. 7C). 1555

Journal of Cell Science (2017) 130, 2551-2563 doi:10.1242/jcs.200642

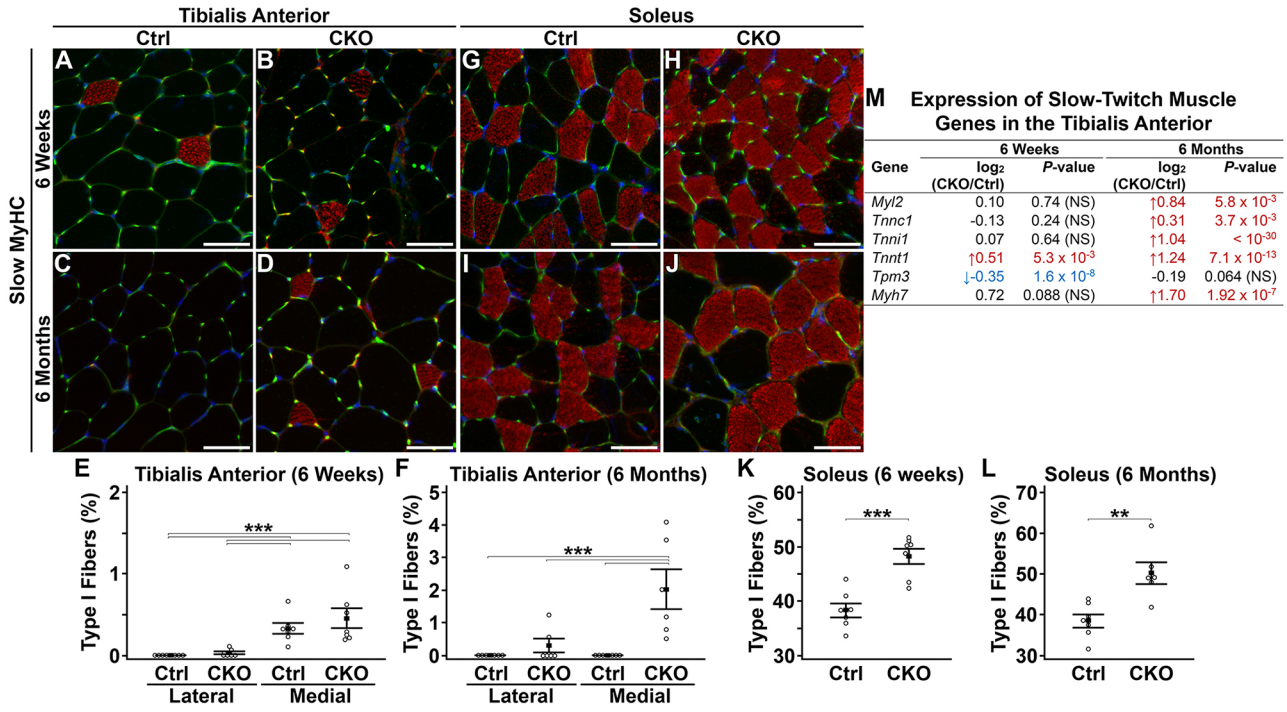

M Expression of Slow-Twitch Muscle Genes in the Tibialis Anterior

Gene	6 Weeks log2 (CKO/Ctrl)	6 Weeks P-value	6 Months log2 (CKO/Ctrl)	6 Months P-value
Myl2	0.10	0.74 (NS)	↑0.84	5.8×10^{-3}
Tnnc1	-0.13	0.24 (NS)	↑0.31	3.7×10^{-3}
Tnni1	0.07	0.64 (NS)	↑1.04	$< 10^{-30}$
Tnnt1	↑0.51	5.3×10^{-3}	↑1.24	7.1×10^{-13}
Tpm3	↓-0.35	1.6×10^{-8}	-0.19	0.064 (NS)
Myh7	0.72	0.088 (NS)	↑1.70	1.92×10^{-7}

Fig. 6. Increased abundance of type I fibers. (A–J) Immunofluorescence for MYH7 (slow MyHC) in the TA (A–D) or soleus (G–J). Red, slow MyHC; green, membranes stained with WGA-488; blue, nuclei stained with DAPI. In the TA, no differences were observed in the percentage of type I fibers at 6 weeks of age; however, the medial region exhibited more type I fibers than the lateral region. ***P<0.001 (Kruskal–Wallis test, n=7 animals/group) (E). At 6 months, *Hira* CKO mice exhibited more type I fibers in the medial TA (***P<0.001, Kruskal–Wallis test, n=6 animals/group) (F). *Hira* CKO mice exhibited significantly more type I fibers than controls in the soleus at both 6 weeks (K) and 6 months (L) of age. **P<0.01, ***P<0.001 (Student's t-test; 6 weeks, n=7 animals/group; 6 months, n=7 Ctrl and 6 CKO animals/group). (M) Microarray results for expression of slow-twitch muscle genes. Slow-twitch isoforms were mostly unchanged at 6 weeks of age, but upregulated at 6 months of age. Error bars show the mean±s.e.m. Scale bars: 50 µm.

genes were commonly downregulated in the two *Hira* CKOs (Fig. 7B). Gene Ontology analysis showed enrichment of genes involved in DNA repair, transcription and response to cellular stress (Fig. 7C). These data support the conclusion we reached after analysis of mice lacking HIRA in cardiomyocytes, which is that HIRA deficiency impairs expression of cellular stress response genes leaving myocytes susceptible to DNA lesions and damage by ROS.

DISCUSSION

Previous work has revealed important roles for HIRA in myogenesis. It is important for the differentiation of C2C12 myoblasts into myotubes (Song et al., 2012). HIRA facilitates expression of *Myod1* through incorporation of histone H3.3 into its promoter and enhancer regions (Yang et al., 2011b). Histone H3.3 itself epigenetically maintains expression of the *Myod1* gene after cell division (Ng and Gurdon, 2008). HIRA cooperates with MEF2 transcription factors to drive expression of MEF2 target genes, like *Myog* (Yang et al., 2011a). HIRA is also a substrate for AKT proteins. HIRA phosphorylation by AKT proteins in myoblasts preserves the proliferative state. Dephosphorylation occurs as myoblasts differentiate towards myotubes (Yang et al., 2016). Thus, HIRA-mediated chromatin assembly is critical during myogenesis. In this study, we expanded our understanding of the function of HIRA in skeletal muscle by determining the consequence of its loss after myogenesis in the homeostasis and function of postmitotic muscle fibers.

Mice lacking HIRA in skeletal muscle exhibited lower body weight, less fat mass and increased lean mass as a percentage of body weight. There was no difference in mass for any individual muscle; therefore, the increase in percentage lean mass is best explained by the reduction of total body fat. Reduced body fat probably accounts for the observed lower body weight as well. Reduced fat mass could be due to increased oxidative metabolism due to more type I fibers or increased energy demand from hypertrophic fibers. The *Hira* CKO is specific to myofibers, so the effect on fat mass must be an indirect consequence of altered muscle metabolism.

The hypertrophic response to loss of HIRA appears to affect type II fibers much more profoundly. The increase in myofibers with central nuclei in the soleus was very modest. In contrast, the TA muscle of *Hira* CKO mice had 15% of fibers with central nuclei. Similar to the *Hira* CKO, deletion of the muscle-specific lysine methyltransferase *Smyd1* produced a phenotype that was prevalent in the TA muscle, but not the soleus, and included upregulation of genes involved in muscle growth and development (Stewart et al., 2016). Although these results are only correlative, similarities between these two CKOs suggest that fast-twitch muscles might be more susceptible to stress-induced damage and misregulation of gene expression as a consequence of epigenetic perturbations. This observed difference between fast- and slow-twitch muscles supports the link between hypertrophy and regeneration. Hypertrophy was undetectable, and there were very few fibers with central nuclei in soleus; whereas, there was pronounced hypertrophy and high numbers of fibers with central nuclei in the TA. These observations suggested to us that the hypertrophic fibers in the *Hira* CKO ultimately degenerate, stimulating regeneration in those areas.

There is little data in the literature supporting a relationship between HIRA and muscle hypertrophy. HIRA interacts with the transcription factor RUNX1. RUNX1 promotes muscle growth, preserves myofibrillar stability and prevents muscle wasting/atrophy

Journal of Cell Science (2017) 130, 2551-2563 doi:10.1242/jcs.200642

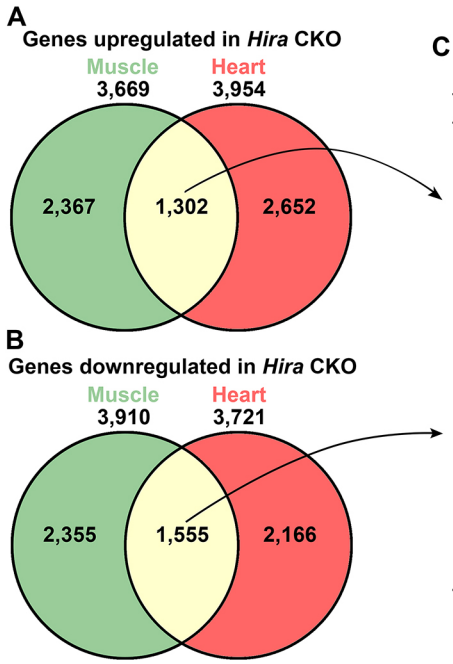

C

GO terms common to both skeletal muscle and cardiomyocyte *Hira* CKOs

Rank	GO term (biological processes)	*P*-value	FDR
Upregulated genes			
1	Translation	4.09×10^{-8}	4.15×10^{-6}
2	Protein localization	1.23×10^{-6}	6.24×10^{-5}
3	Protein transport	1.16×10^{-5}	3.92×10^{-4}
4	Establishment of protein localization	1.50×10^{-5}	4.35×10^{-4}
5	Cell proliferation	2.81×10^{-5}	6.34×10^{-4}
Downregulated genes			
1	DNA repair	1.31×10^{-5}	3.34×10^{-4}
2	DNA metabolic process	1.88×10^{-5}	3.88×10^{-4}
3	Transcription	1.98×10^{-5}	3.88×10^{-4}
4	Response to DNA damage stimulus	2.82×10^{-5}	4.79×10^{-4}
5	Regulation of transcription	3.18×10^{-5}	4.85×10^{-4}
6	Cellular response to stress	9.19×10^{-5}	1.02×10^{-3}
7	Chromatin modification	1.12×10^{-4}	1.19×10^{-3}
8	Chromosome organization	1.75×10^{-4}	1.72×10^{-3}
9	tRNA metabolic process	1.89×10^{-4}	1.79×10^{-3}
10	Oxidation reduction	2.45×10^{-4}	2.15×10^{-3}
11	Chromatin organization	4.53×10^{-4}	3.73×10^{-3}

Fig. 7. Similarities in differential gene expression between muscle and heart. Identification and analysis of genes that were differentially expressed in both *Hira* CKO cardiomyocytes and *Hira* CKO skeletal myocytes. Data were obtained by microarray analysis. Groups were: (1) left ventricle of *Hira* CKO using *αMyHC-cre*, (2) left ventricle of control littermates, (3) TA of *Hira* CKO using *Myf6-cre*, and (4) TA of control littermates (n=4 animals/group). (A,B) Venn diagrams illustrating the number of common differentially-expressed genes upregulated (A) or downregulated (B) in both *Hira* CKO heart and skeletal muscle. (C) Significantly-enriched Gene Ontology (GO) terms for shared differentially expressed genes ranked by *P*-value. Only those GO terms with $P<0.0001$ and FDR<0.001 are shown. This analysis illustrates an important role for HIRA in transcriptional responses to cellular stresses such as DNA damage and reactive oxygen species.

(Wang et al., 2005). HIRA interacts with RUNX1 and facilitates expression of RUNX1 target genes in hematopoietic stem cells. HIRA also regulates expression of *Runx1* itself by mediating H3.3 incorporation at the *Runx1* promoter/enhancer region. HIRA is essential for *Runx1* expression during the endothelial to hematopoietic transition (Majumder et al., 2015). Our microarray analysis showed expression of *Runx1* to be higher at both 6 weeks and 6 months in *Hira* CKO skeletal muscle relative to control mice. Thus, upregulation of *Runx1* in *Hira* CKO myocytes could contribute to hypertrophy.

HIRA also interacts with the anti-proliferative protein prohibitin (PHB), which stabilizes the association of the HIRA complex with certain gene promoters (Zhu et al., 2017). In rat cardiac muscle, reduced PHB contributes to left ventricular hypertrophy (Zheng and Lu, 2015). Reduced PHB protein was also the major finding in a biomarker study of cardiac hypertrophy in rats (Chowdhury et al., 2013). Presumably, disruption of HIRA recruitment to gene promoters contributes to the PHB deficiency phenotype. Deficiency in either HIRA or PHB might cause similar gene expression alterations that lead to hypertrophy of striated muscle. It would be interesting to determine whether hypertrophy resulting from PHB deficiency is a consequence of impaired responses to oxidative stress.

We also observed increased numbers of type I myofibers in *Hira* CKO mice. This was especially true for the soleus, where the percentage of type I fibers had increased by 25%. This is despite the observation that the pathology was modest for the soleus. We are still left questioning why fiber type switching would occur in our myofiber *Hira* CKO. *Hira* was deleted from myofibers, not myoblasts. Thus, our CKO should not affect myoblast differentiation. These data support the idea that HIRA impacts myofiber energy metabolism, which could account for the lean phenotype in *Hira* CKO mice. Note that many of the Gene Ontology terms associated with differentially expressed genes in the *Hira* CKO at 6 months of age relate to metabolic processes (Table 1), further supporting this idea.

A goal of this study was to identify genes and pathways that were impacted by HIRA deficiency in both cardiac and skeletal muscle using data from our previous investigation of *Hira* deletion in cardiomyocytes (Valenzuela et al., 2016). With this comparison, we hoped to identify pathways that were particularly affected by loss of HIRA. Both *Hira* CKO cardiomyocytes and skeletal myofibers exhibited hypertrophy, sarcolemmal damage, upregulation of fetal/developmental genes and downregulation of genes associated with responses to cellular stresses and DNA damage.

Hypertrophy appears to be a default consequence of HIRA deficiency in striated muscle, as it was observed for both *Hira* CKO myofibers and cardiomyocytes. The hypertrophic myofibers and cardiomyocytes in both *Hira* CKO mouse models become susceptible to degeneration as evident by Evans Blue dye uptake and accumulation of nitrotyrosine. In the heart, these cells are replaced with fibrotic lesions (Valenzuela et al., 2016). In skeletal muscle, they simply degenerate and are replaced with new fibers. Expression of regeneration-associated genes in the *Hira* CKO TA muscle was obvious, but newly formed eMyHC-positive fibers were rare. This could indicate that fusion of myoblasts with existing fibers for repair is more prevalent than *de novo* fiber formation. Elevated expression of growth, fetal and developmental genes was observed in both *Hira* CKO skeletal and cardiac muscle. Thus, hypertrophy could be a consequence of increased expression of genes associated with muscle development. These gene expression changes are likely caused by impaired replication-independent assembly of nucleosomes containing H3.3, which leads to abnormal transcriptional regulation of muscle genes. Fetal and developmental genes might not be properly silenced in the absence of HIRA. HIRA

Journal of Cell Science (2017) 130, 2551-2563 doi:10.1242/jcs.200642

might also affect transcription levels, leading to higher than normal production of muscle genes in its absence. Supporting a role for HIRA in transcriptional regulation of striated muscle genes, HIRA facilitates H3.3 incorporation into enhancers for the cardiac transcription factor Nkx2.5 during embryonic development and, depending on gene context, has positive or negative effects on cardiac gene expression (Dilg et al., 2016).

Interestingly, genes associated with responses to oxidative stress and DNA repair were downregulated in both the *Hira* heart and skeletal muscle CKOs. These genes were downregulated despite evidence for increased oxidative stress. By its nature, skeletal muscle produces free radicals that, if not neutralized, can cause oxidative damage to intracellular components (Davies et al., 1982; Powers and Jackson, 2008). Our gene expression data point to impaired transcriptional responses to cellular stress and DNA damage, meaning that *Hira* CKO myocytes might be susceptible to oxidative damage and DNA lesions because they are unable to upregulate expression of genes to cope with or repair the damage. For DNA damage, a failed transcriptional response is likely exacerbated by the already low efficiency of DNA base excision repair in myocytes (Narciso et al., 2007). The fact that oxidative stress to DNA, lipids and proteins in myocytes increases with age (Fano et al., 2001; Mecocci et al., 1999; Pansarasa et al., 1999, 2000) could explain why the *Hira* CKO phenotype was substantial at 6 months of age, but weak at 6 weeks of age. Collectively, these data suggest that loss of HIRA impairs transcriptional responses to cellular stress, leaving myocytes vulnerable to oxidative stress-induced damage and DNA lesions.

In this model, HIRA is eliminated from myofibers at inception (myotube stage); therefore, the observed phenotype is the cumulative effect of physiological changes that occurred over the life of the fiber. We examined the phenotype of *Hira* CKO at two time points, 6 weeks and 6 months of age. At 6 weeks of age, mice are reproductively mature, but are still growing. Six-month-old mice are considered middle-aged, growth has stopped and fat accumulation will occur depending on diet and exercise. We limited this study to just two time points because of the high cost and effort it takes for phenotypic and gene expression analyses at each time point. Because this was not a longitudinal study with periodic analysis over time, we cannot determine the precise time at which defects begin to occur. It is possible that muscle growth (as is occurring at 6 weeks) masks the pathological peculiarities and misregulation of gene expression observed at 6 months.

There is a relationship between HIRA and production of NADPH, perturbation of which might contribute to susceptibility to oxidative stress. NADPH provides the reducing equivalents to regenerate antioxidants like glutathione and thioredoxin. As mentioned above, The HIRA complex interacts with PHB, which functions to stabilize its association with many gene promoters (Zhu et al., 2017). In embryonic stem cells, PHB-containing HIRA complexes promote transcription of the isocitrate dehydrogenase genes (*Idh1* and *Idh2*), which generate NADPH. Our results are consistent with this model in that expression of both *Idh1* and *Idh2* was downregulated in *Hira* CKO skeletal muscle at 6 months of age. Furthermore, glutathione-disulfide reductase (*Gsr*), the enzyme that uses NADPH to regenerate glutathione, was also downregulated in the *Hira* CKO mice.

MATERIALS AND METHODS

Animals

Hira$^{tm1a(EUCOMM)Wtsi}$ (knockout first gene trap) mice were obtained from the European Mouse Mutant Archive (EMMA, stock #EM:05901). *Rosa26*$^{YFP/YFP}$ and *Myf6*$^{cre/cre}$ mice were obtained from the Jackson Laboratory (stock #7903 and #10528, respectively). The *Hira*^{flox} allele was generated by crossing *Hira*$^{tm1a(EUCOMM)Wtsi}$ to *Rosa26*$^{FLP/FLP}$ (Flipper) (Jackson Laboratory, stock #9086). *Hira*$^{+/-}$ were generated by crossing *Hira*$^{flox/+}$ to the maternal deleter *Tg(Sox2-cre)* (Jackson Laboratory, stock #8454). Experimental animals were generated by crossing *Myf6*$^{cre/+}$; *Hira*$^{flox/-}$ mice to *Hira*$^{flox/flox}$; *Rosa26*$^{YFP/YFP}$ mice. Controls were *Myf6*$^{cre/+}$; *Hira*$^{flox/+}$; *Rosa26*$^{YFP/+}$. *Hira* CKOs were *Myf6*$^{cre/+}$; *Hira*$^{flox/-}$; *Rosa26*$^{YFP/+}$.

The following primers were used for genotyping: Cre-F, 5′-GCCACC-AGCCAGCTATCAACTC-3′ and Cre-R, 5′-TTGCCCCTGTTTCACTAT-CCAG-3′; Hira-F, 5′-CCTTCCTCTGCTTTGTTTGTTC-3′ and Hira-R2, 5′-CCACCGCACACAGTTCACAC-3′ with Hira-R3, 5′-GCCAAGTGA-GCACAGAAGATGG-3′. Hira-F and Hira-R2 identifies wild-type and flox alleles (691 bp and 783 bp, respectively). Hira-F and Hira-R3 identifies the null allele (587 bp). All experimental procedures involving mice were approved by the Institutional Animal Care and Use Committee of the University of Houston.

Body composition

Body composition (percentage fat and lean mass) was calculated by magnetic resonance imaging (MRI) using an Echo MRI system (Echo Medical Systems, Houston, TX).

Strength and motor coordination tests

Strength was assayed by a grip strength test. The device consisted of a scale attached to a wire mesh. The scale was immobilized and grip strength was measured by allowing the mouse to grasp the wire mesh with all four paws and then pulling the tail with increasing force until it releases its grip. The test was repeated three times per mouse with a 15 s interval between tests. Data reported is the maximum pull of the three trials.

Tissue collections

Immediately after euthanasia, measurements were obtained for body weight and length followed by dissection of muscles in PBS. Excess PBS was removed by blotting on a paper towel. Muscles were weighed in pairs using an analytical scale (Denver Instrument, model# SI-114). For RNA extraction, tissues were snap frozen in liquid nitrogen and stored at −80C. For H&E staining, immunofluorescence and Evans Blue dye visualization, fluorescence tissues were snap frozen in liquid nitrogen-cooled isopentane and stored at −80C until preparation of cryosections.

Histology and immunofluorescence

H&E staining was performed by standard methods using 7 µm cryosections. Immunofluorescence was performed on 7 µm cryosections using antibodies for eMyHC (1:40; Developmental Studies Hybridoma Bank, clone F1.652), nitrotyrosine (1:200; Santa Cruz Biotechnology, cat #sc-32757) or slow/β-MyHC (against MYH7; 1:40; clone A4.840, deposited to the Developmental Studies Hybridoma Bank by H. M. Blau). Sections were blocked and antibodies diluted using 1× casein and 2% normal serum in phosphate-buffered saline with 0.1% Tween 20 (PBST) (10× casein stock and normal serum were from Vector Laboratories, Burlingame, CA). Primary antibodies were incubated overnight at 4°C. Secondary antibodies were incubated for 1 h at room temperature. Slides were stained with DAPI during washing, and coverslips mounted with Vectashield HardSet mounting medium (Vector Laboratories).

Central nuclei and minimum Feret diameter measurements

The percentage of myofibers with centralized nuclei was determined by manual counting. Data were derived from 20× composite fluorescence images (large scan) of wheat germ agglutinin (WGA) conjugated to Alexa Fluor 488 (Thermo Fisher Scientific, cat #W11261). The number of fibers exhibiting centralized (internal) nuclei was divided by the total number of fibers in each image (soleus, 153–716 and 190–537 fibers/animal at 6 weeks and 6 months, respectively; TA medial, 314–1115 and 384–876 fibers/animal at 6 weeks and 6 months, respectively; TA lateral, 293–1108 and 302–468 fibers/animal at 6 weeks and 6 months, respectively).

Myofiber minimum Feret diameter was calculated by using the analyze particles tool of ImageJ software. Data were derived from 20× composite WGA-488 fluorescence images (soleus, 117–370 and 137–430 fibers/animal at 6 weeks and 6 months, respectively; TA medial, 205–653 and 323–775 fibers/animal at 6 weeks and 6 months, respectively; TA lateral, 100–600 and 213–380 fibers/animal at 6 weeks and 6 months, respectively).

Evans Blue dye uptake assay

To assay sarcolemmal integrity, mice were exercised for 30 min on a treadmill (12 m/min, 5% incline) and then given an intraperitoneal injection of Evans Blue dye (5 µl of 1% solution in PBS/g body weight). Mice were euthanized 18 h later for tissue collection. Evans Blue dye staining was viewed as far-red fluorescence in 7 µm cryosections.

Microscopy

Brightfield and epifluorescence images of tissue sections were obtained using a Nikon Ti-E inverted microscope equipped with a DS-Fi1 5-megapixel color camera (Nikon Instruments), a CoolSNAP HQ2 14-bit monochrome camera (Photometrics, Tucson, AZ) and NIS Elements software v4.13 (Nikon Instruments). Stereoimages (brightfield and fluorescence) were captured with a Leica MZ10F stereomicroscope and the extended depth of focus feature of LAS v3.7 software (Leica Microsystems, Wetzlar, Germany).

Reverse transcription PCR

Total RNA was extracted from TA muscles using TRIzol reagent (ThermoFisher Scientific). cDNA was prepared from this RNA using a SuperScript II reverse transcription kit (ThermoFisher) according to the manufacturer's recommendations. Primers that flanked exon 4 of the *Hira* cDNA were: 5′-TTCCCAAGATGCTTTGCCAG-3′ and 5′-CGATCATC-AGCTTGAGAGGC-3′. Expected product sizes were 412 bp for wild-type and 321 bp for the deleted allele. Primers for *Actb* (β-actin) were: 5′-AA-AGACCTCTATGCCAACACAGTGC-3′ and 5′-GTACTCCTGCTTGCT-GATCCACATC-3′. Expected product size was 216 bp.

qPCR

Total RNA for qPCR was extracted using TRIzol reagent according to the manufacturer's instructions (ThermoFisher Scientific, Waltham, MA). Relative mRNA levels were measured using TaqMan gene expression assays with 6-carboxyfluorescein (FAM)-labeled probes. Primer probe sets were: Mm01332463_m1 for *Myh3* (ThermoFisher Scientific) and *Gapdh* (Gapdh-F, 5′-ACTGGCATGGCCTTCCG-3′; Gapdh-R, 5′-CAGGCGGC-ACGTCAGATC-3′; Gapdh-Probe, 5′-TTCCTACCCCCAATGTGTCCG-TCGT-3′) (Biosearch Technologies, Petaluma, CA). *Gapdh* mRNA expression levels were used for normalization. The PCR was run using an ABI Prism 7900HT thermocycler and SDS2.1 software (Applied Biosystems). Data were analyzed by the comparative ΔΔCt method.

Microarrays

Total RNA for microarray analysis was extracted from the TA muscle of 6-week- and 6-month-old mice (n=4 mice per group) using TRIzol reagent (ThermoFisher Scientific) according to the manufacturer's instructions. Each sample was hybridized to triplicate arrays. Gene expression profiling and data analysis was performed using the MouseOne Array Plus v2.1 service from Phalanx Biotech (Palo Alto, CA). Raw intensity data was normalized using the median scaling normalization method. Normalized spot intensities were transformed into gene expression log2 ratios. A P-value of less than 0.05 was used to identify differentially expressed genes. Based on the log2 fold change, we selected 1000 differentially expressed genes (500 from upregulated and 500 from downregulated sets). Clustering analysis was performed using these 1000 differentially expressed genes. An unsupervised hierarchical clustering analysis on these 1000 genes revealed that samples representing the treatment and control conditions grouped together. Principal component analysis (PCA) was also performed on this subset of genes to evaluate any differences among biological replicates and their treatment conditions. Gene Ontology (GO) analyses were performed using DAVID (https://david.ncifcrf.gov/). Enriched GO terms were ranked by P-value. To adjust for multiple testing for individual GO terms, a false discovery rate (FDR) value for each term was calculated (Benjamini and Hochberg, 1995). GO terms with an FDR<0.001 were reported. The 6-week and 6-month datasets were deposited into the NCBI Gene Expression Omnibus (GEO) database under series accession numbers GSE97359 (https://www.ncbi.nlm.nih.gov/geo/query/acc.cgi?acc=GSE97359) and GSE90900 (https://www.ncbi.nlm.nih.gov/geo/query/acc.cgi?acc=GSE90900), respectively.

Reverse phase protein array

Protein lysates from the TA muscle of 6-month-old male mice were prepared by homogenization in T-PER buffer (ThermoFisher Scientific) supplemented with protease and phosphatase inhibitors. Protein lysates were quantified, and protein arrays were printed and stained as described previously (Byers et al., 2012). Images were quantified with MicroVigene 4.0 (VigeneTech, Carlisle, MA). The spot-level raw data were processed with the R package SuperCurve suite, which returns the estimated protein concentration (raw concentration) and a quality control score for each slide, as described previously (Byers et al., 2012). Only slides with a quality control score of >0.8 were used for downstream analysis. The raw concentration data were normalized by median-centering each sample across all the proteins to correct loading bias.

Statistical analyses

Statistical tests were conducted by using MedCalc v14.12.0 software (MedCalc Software bvba, Belgium). For studies with two experimental groups, an independent samples Student's t-test was performed. For experiments with more than two experimental groups, quantitative data were subjected to one-way analysis of variance (ANOVA). If the ANOVA was positive (P<0.05), a post-hoc Student–Newman–Keuls test was performed for pairwise comparison of subgroups. Prior to the ANOVA test, Levene's test for equality of variances was performed. If the Levene test was positive (P<0.05) then a logarithmic transformation was applied and the test was repeated. If Levene's test was still positive after logarithmic transformation, the non-parametric Kruskal–Wallis test was used in place of the ANOVA. Two-way ANOVA was used for minimum Feret diameter data. A P-value of <0.05 was considered significant for all tests.

Acknowledgements

The authors thank Dr C. Allison Stewart (M.D. Anderson Cancer Center) for editorial assistance and insightful suggestions. The authors thank Wei Yu (University of Houston) for technical assistance.

Competing interests

The authors declare no competing or financial interests.

Author contributions

Conceptualization: N.V., R.J.S., M.S.; Methodology: N.V., M.S.; Software: B.S.; Formal analysis: N.V., B.S., L.L., J.W., M.S.; Investigation: N.V., M.S.; Resources: J.W., L.A.B., Y.L., R.J.S., M.S.; Data curation: B.S., L.L., J.W.; Writing - original draft: M.S.; Writing - review & editing: M.S.; Supervision: J.W., L.A.B., R.J.S., M.S.; Project administration: M.S.; Funding acquisition: B.S., L.A.B., Y.L., R.J.S., M.S.

Funding

This work was supported by the American Heart Association (12BGIA11860006 to M.D.S., and 11SDG5260033 and 16GRNT27760164 to Y.L.), the Texas Heart Institute (to M.D.S. and R.J.S.), the University of Houston-Downtown Organized Research and Creative Activities Grant (to B.S.), an University of Texas MD Anderson Cancer Center Physician Scientist Award (to L.A.B.), and the Sheikh Khalifa Bin Zayed Al Nahyan Institute for the Personalized Cancer Therapy's (IPCT's) Center for Professional Education and Training (to L.A.B.).

Data availability

The microarray datasets from 6-week-old and 6-month-old mice were deposited into the NCBI Gene Expression Omnibus (GEO) database under series accession numbers GSE97359 (https://www.ncbi.nlm.nih.gov/geo/query/acc.cgi?acc=GSE97359) and GSE90900 (https://www.ncbi.nlm.nih.gov/geo/query/acc.cgi?acc=GSE90900), respectively.

Supplementary information

Supplementary information available online at http://jcs.biologists.org/lookup/doi/10.1242/jcs.200642.supplemental

References

Adam, S., Polo, S. E. and Almouzni, G. (2013). Transcription recovery after DNA damage requires chromatin priming by the H3.3 histone chaperone HIRA. *Cell* **155**, 94-106.

Ahmad, K. and Henikoff, S. (2002a). Histone H3 variants specify modes of chromatin assembly. *Proc. Natl. Acad. Sci. USA* **99**, 16477-16484.

Ahmad, K. and Henikoff, S. (2002b). The histone variant H3.3 marks active chromatin by replication-independent nucleosome assembly. *Mol. Cell* **9**, 1191-1200.

Banaszynski, L. A., Wen, D., Dewell, S., Whitcomb, S. J., Lin, M., Diaz, N., Elsasser, S. J., Chapgier, A., Goldberg, A. D., Canaani, E. et al. (2013). Hira-dependent histone H3.3 deposition facilitates PRC2 recruitment at developmental loci in ES cells. *Cell* **155**, 107-120.

Benjamini, Y. and Hochberg, Y. (1995). Controlling the false discovery rate - a practical and powerful approach to multiple testing. *J. R. Stat. Soc. Series B Methodol.* **57**, 289-300.

Burgess, R. J. and Zhang, Z. (2013). Histone chaperones in nucleosome assembly and human disease. *Nat. Struct. Mol. Biol.* **20**, 14-22.

Byers, L. A., Wang, J., Nilsson, M. B., Fujimoto, J., Saintigny, P., Yordy, J., Giri, U., Peyton, M., Fan, Y. H., Diao, L. et al. (2012). Proteomic profiling identifies dysregulated pathways in small cell lung cancer and novel therapeutic targets including PARP1. *Cancer Discov.* **2**, 798-811.

Carlson, C., Sirotkin, H., Pandita, R., Goldberg, R., McKie, J., Wadey, R., Patanjali, S. R., Weissman, S. M., Anyane-Yeboa, K., Warburton, D. et al. (1997). Molecular definition of 22q11 deletions in 151 velo-cardio-facial syndrome patients. *Am. J. Hum. Genet.* **61**, 620-629.

Chowdhury, D., Tangutur, A. D., Khatua, T. N., Saxena, P., Banerjee, S. K. and Bhadra, M. P. (2013). A proteomic view of isoproterenol induced cardiac hypertrophy: prohibitin identified as a potential biomarker in rats. *J. Transl. Med.* **11**, 130.

Davies, K. J. A., Quintanilha, A. T., Brooks, G. A. and Packer, L. (1982). Free radicals and tissue damage produced by exercise. *Biochem. Biophys. Res. Commun.* **107**, 1198-1205.

Dilg, D., Saleh, R. N. M., Phelps, S. E. L., Rose, Y., Dupays, L., Murphy, C., Mohun, T., Anderson, R. H., Scambler, P. J. and Chapgier, A. L. A. (2016). HIRA is required for heart development and directly regulates Tnni2 and Tnnt3. *PLoS ONE* **11**, e0161096.

Drane, P., Ouararhni, K., Depaux, A., Shuaib, M. and Hamiche, A. (2010). The death-associated protein DAXX is a novel histone chaperone involved in the replication-independent deposition of H3.3. *Genes Dev.* **24**, 1253-1265.

Fano, G., Mecocci, P., Vecchiet, J., Belia, S., Fulle, S., Polidori, M. C., Felzani, G., Senin, U., Vecchiet, L. and Beal, M. F. (2001). Age and sex influence on oxidative damage and functional status in human skeletal muscle. *J. Muscle Res. Cell Motil.* **22**, 345-351.

Gaume, X. and Torres-Padilla, M.-E. (2015). Regulation of reprogramming and cellular plasticity through histone exchange and histone variant incorporation. *Cold Spring Harb. Symp. Quant. Biol.* **80**, 165-175.

Goldberg, A. D., Banaszynski, L. A., Noh, K.-M., Lewis, P. W., Elsaesser, S. J., Stadler, S., Dewell, S., Law, M., Guo, X., Li, X. et al. (2010). Distinct factors control histone variant H3.3 localization at specific genomic regions. *Cell* **140**, 678-691.

Gurard-Levin, Z. A., Quivy, J.-P. and Almouzni, G. (2014). Histone chaperones: assisting histone traffic and nucleosome dynamics. *Annu. Rev. Biochem.* **83**, 487-517.

Halford, S., Wadey, R., Roberts, C., Daw, S. C. M., Whiting, J. A., O'Donnell, H., Dunham, I., Bentley, D., Lindsay, E., Baldini, A. et al. (1993). Isolation of a putative transcriptional regulator from the region of 22q11 deleted in DiGeorge syndrome, Shprintzen syndrome and familial congenital heart disease. *Hum. Mol. Genet.* **2**, 2099-2107.

Hamiche, A. and Shuaib, M. (2012). Chaperoning the histone H3 family. *Biochim. Biophys. Acta* **1819**, 230-237.

Lewis, P. W., Elsaesser, S. J., Noh, K.-M., Stadler, S. C. and Allis, C. D. (2010). Daxx is an H3.3-specific histone chaperone and cooperates with ATRX in replication-independent chromatin assembly at telomeres. *Proc. Natl. Acad. Sci. USA* **107**, 14075-14080.

Majumder, A., Syed, K. M., Joseph, S., Scambler, P. J. and Dutta, D. (2015). Histone chaperone HIRA in regulation of transcription factor RUNX1. *J. Biol. Chem.* **290**, 13053-13063.

Mecocci, P., Fano, G., Fulle, S., MacGarvey, U., Shinobu, L., Polidori, M. C., Cherubini, A., Vecchiet, J., Senin, U. and Beal, M. F. (1999). Age-dependent increases in oxidative damage to DNA, lipids, and proteins in human skeletal muscle. *Free Radic. Biol. Med.* **26**, 303-308.

Narciso, L., Fortini, P., Pajalunga, D., Franchitto, A., Liu, P., Degan, P., Frechet, M., Demple, B., Crescenzi, M. and Dogliotti, E. (2007). Terminally differentiated muscle cells are defective in base excision DNA repair and hypersensitive to oxygen injury. *Proc. Natl. Acad. Sci. USA* **104**, 17010-17015.

Ng, R. K. and Gurdon, J. B. (2008). Epigenetic memory of an active gene state depends on histone H3.3 incorporation into chromatin in the absence of transcription. *Nat. Cell Biol.* **10**, 102-109.

Pansarasa, O., Bertorelli, L., Vecchiet, J., Felzani, G. and Marzatico, F. (1999). Age-dependent changes of antioxidant activities and markers of free radical damage in human skeletal muscle. *Free Radic. Biol. Med.* **27**, 617-622.

Pansarasa, O., Castagna, L., Colombi, B., Vecchiet, J., Felzani, G. and Marzatico, F. (2000). Age and sex differences in human skeletal muscle: role of reactive oxygen species. *Free Radic. Res.* **33**, 287-293.

Powers, S. K. and Jackson, M. J. (2008). Exercise-induced oxidative stress: cellular mechanisms and impact on muscle force production. *Physiol. Rev.* **88**, 1243-1276.

Rai, T. S. and Adams, P. D. (2012). Lessons from senescence: chromatin maintenance in non-proliferating cells. *Biochim. Biophys. Acta* **1819**, 322-331.

Schwartz, B. E. and Ahmad, K. (2005). Transcriptional activation triggers deposition and removal of the histone variant H3.3. *Genes Dev.* **19**, 804-814.

Song, T.-Y., Yang, J.-H., Park, J. Y., Song, Y., Han, J.-W., Youn, H.-D. and Cho, E.-J. (2012). The role of histone chaperones in osteoblastic differentiation of C2C12 myoblasts. *Biochem. Biophys. Res. Commun.* **423**, 726-732.

Stewart, M. D., Lopez, S., Nagandla, H., Soibam, B., Benham, A., Nguyen, J., Valenzuela, N., Wu, H. J., Burns, A. R., Rasmussen, T. L. et al. (2016). Mouse myofibers lacking the SMYD1 methyltransferase are susceptible to atrophy, internalization of nuclei and myofibrillar disarray. *Dis. Model. Mech.* **9**, 347-359.

Tagami, H., Ray-Gallet, D., Almouzni, G. and Nakatani, Y. (2004). Histone H3.1 and H3.3 complexes mediate nucleosome assembly pathways dependent or independent of DNA synthesis. *Cell* **116**, 51-61.

Udugama, M., FT, M. C., Chan, F. L., Tang, M. C., Pickett, H. A., JD, R. M., Mayne, L., Collas, P., Mann, J. R. and Wong, L. H. (2015). Histone variant H3.3 provides the heterochromatic H3 lysine 9 tri-methylation mark at telomeres. *Nucleic Acids Res.* **43**, 10227-10237.

Valenzuela, N., Fan, Q., Fa'ak, F., Soibam, B., Nagandla, H., Liu, Y., Schwartz, R. J., McConnell, B. K. and Stewart, M. D. (2016). Cardiomyocyte-specific conditional knockout of the histone chaperone HIRA in mice results in hypertrophy, sarcolemmal damage and focal replacement fibrosis. *Dis. Model. Mech.* **9**, 335-345.

Venkatesh, S. and Workman, J. L. (2015). Histone exchange, chromatin structure and the regulation of transcription. *Nat. Rev. Mol. Cell Biol.* **16**, 178-189.

Wang, X., Blagden, C., Fan, J., Nowak, S. J., Taniuchi, I., Littman, D. R. and Burden, S. J. (2005). Runx1 prevents wasting, myofibrillar disorganization, and autophagy of skeletal muscle. *Genes Dev.* **19**, 1715-1722.

Wong, L. H., Ren, H., Williams, E., McGhie, J., Ahn, S., Sim, M., Tam, A., Earle, E., Anderson, M. A., Mann, J. et al. (2009). Histone H3.3 incorporation provides a unique and functionally essential telomeric chromatin in embryonic stem cells. *Genome Res.* **19**, 404-414.

Yang, J.-H., Choi, J.-H., Jang, H., Park, J.-Y., Han, J.-W., Youn, H.-D. and Cho, E.-J. (2011a). Histone chaperones cooperate to mediate Mef2-targeted transcriptional regulation during skeletal myogenesis. *Biochem. Biophys. Res. Commun.* **407**, 541-547.

Yang, J.-H., Song, Y., Seol, J.-H., Park, J. Y., Yang, Y.-J., Han, J.-W., Youn, H.-D. and Cho, E.-J. (2011b). Myogenic transcriptional activation of MyoD mediated by replication-independent histone deposition. *Proc. Natl. Acad. Sci. USA* **108**, 85-90.

Yang, J.-H., Song, T.-Y., Jo, C., Park, J., Lee, H.-Y., Song, I., Hong, S., Jung, K. Y., Kim, J., Han, J.-W. et al. (2016). Differential regulation of the histone chaperone HIRA during muscle cell differentiation by a phosphorylation switch. *Exp. Mol. Med.* **48**, e252.

Zhang, R., Poustovoitov, M. V., Ye, X., Santos, H. A., Chen, W., Daganzo, S. M., Erzberger, J. P., Serebriiskii, I. G., Canutescu, A. A., Dunbrack, R. L. et al. (2005). Formation of MacroH2A-containing senescence-associated heterochromatin foci and senescence driven by ASF1a and HIRA. *Dev. Cell* **8**, 19-30.

Zhang, R., Chen, W. and Adams, P. D. (2007). Molecular dissection of formation of senescence-associated heterochromatin foci. *Mol. Cell. Biol.* **27**, 2343-2358.

Zheng, H. and Lu, G. M. (2015). Reduction of prohibitin expression contributes to left ventricular hypertrophy via enhancement of mitochondrial reactive oxygen species formation in spontaneous hypertensive rats. *Free Radic. Res.* **49**, 164-174.

Zhu, Z., Li, C., Zeng, Y., Ding, J., Qu, Z., Gu, J., Ge, L., Tang, F., Huang, X., Zhou, C. et al. (2017). PHB associates with the HIRA complex to control an epigenetic-metabolic circuit in human ESCs. *Cell Stem Cell* **20**, 274-289 e7.

Zink, L.-M. and Hake, S. B. (2016). Histone variants: nuclear function and disease. *Curr. Opin. Genet. Dev.* **37**, 82-89.